Available online at www.sciencedirect.com
SCIENCE DIRECT
Journal of Catalysis 230 (2005) 339–352
JOURNAL OF CATALYSIS
www.elsevier.com/locate/jcat

Effect of cobalt precursor and pretreatment conditions on the structure and catalytic performance of cobalt silica-supported Fischer–Tropsch catalysts

Jean-Sébastien Girardon [a], Anatoly S. Lermontov [a], Léon Gengembre [a], Petr A. Chernavskii [b], Anne Griboval-Constant [a], Andrei Y. Khodakov [a,*]

[a] *Laboratoire de Catalyse de Lille, Université des Sciences et Technologies de Lille, Bât. C3, Cité Scientifique, 59655 Villeneuve d'Ascq, France*
[b] *Department of Chemistry, Moscow State University, 119992 Moscow, Russia*

Received 23 July 2004; revised 9 December 2004; accepted 13 December 2004

Available online 25 January 2005

Abstract

The effect of cobalt precursor and pretreatment conditions on the structure of cobalt species in silica-supported Fischer–Tropsch (FT) catalysts was studied with a combination of characterization techniques (X-ray diffraction, UV–visible, X-ray absorption, X-ray photoelectron spectroscopies, DSC-TGA thermal analysis, propene chemisorption, and temperature-programmed reduction combined with in situ magnetic measurements). The catalysts were prepared via aqueous impregnation of silica with solutions of cobalt nitrate or acetate followed by oxidative pretreatment in air and reduction in hydrogen. It was found that after impregnation and drying cobalt exists in octahedrally coordinated complexes in catalysts prepared from cobalt nitrate or cobalt acetate. Decomposition of the octahedral complexes results in the appearance of Co_3O_4 crystallites and cobalt silicate species. Cobalt repartition between crystalline Co_3O_4 and the cobalt silicate phase in the oxidized samples depends on the exothermicity of salt decomposition in air and the temperature of the oxidative pretreatment. Co_3O_4 crystallite is the dominant phase in the samples prepared via endothermic decomposition of supported cobalt nitrate. Significantly higher cobalt dispersion is found in the catalyst prepared via low-temperature cobalt nitrate decomposition. The uncovered enhanced cobalt dispersion is associated with lower cobalt reducibility. The high exothermicity of cobalt acetate decomposition leads primarily to amorphous, barely reducible cobalt silicate. A more efficient heat flow control at the stage of cobalt acetate decomposition significantly increases the concentration of easy reducible Co_3O_4 in the oxidized catalysts and the number of cobalt metal active sites after reduction. The catalytic measurements show that FT reaction rates depend on the number of cobalt surface metal sites; a higher concentration of cobalt metal sites in the catalysts prepared from cobalt nitrate or with the use of soft cobalt acetate decomposition results in higher catalytic activity in FT synthesis.

Keywords: GTL technology; Fischer–Tropsch synthesis; Cobalt catalysts; Nanoparticles; Cobalt silicate

1. Introduction

The current interest in Fischer–Tropsch (FT) synthesis has largely been driven by the growing demand for clean fuels and the utilization of remote sources of natural and associated gas [1–5]. Supported cobalt catalysts have been particularly attractive for the conversion of synthesis gas to value-added long-chained hydrocarbons, which can be used for the manufacture of diesel or transportation fuels [2–7].

It is known that the catalytic conversion of carbon monoxide occurs on cobalt metal sites situated on the surface of cobalt metal particles dispersed on a porous support. It has been shown that the FT reaction rate is a function of both cobalt dispersion and reducibility. Higher concentrations of cobalt metal sites typically favor higher FT reaction rates [6–10]. The hydrocarbon selectivities generally follow an Anderson–Schulz–Flory (ASF) polymerization se-

* Corresponding author. Fax. +33 3 20 43 65 61.
E-mail address: andrei.khodakov@ec-lille.fr (A.Y. Khodakov).

0021-9517/$ – see front matter
doi:10.1016/j.jcat.2004.12.014

quence with deviations, which are likely to be attributed to the secondary reactions (olefin readsorption, oligomerization, cracking, isomerization) [6,7,10].

Conventional cobalt FT catalysts are prepared via aqueous impregnation of porous oxide supports (silica, alumina, titania, etc.) with solutions of various cobalt salts [7,9–11]. After decomposition of supported cobalt salts via calcination in an oxidizing atmosphere, the catalysts are reduced in hydrogen. Because of a higher surface area, porosity, stability and weak metal–support interaction, silica has been especially convenient for the design of cobalt FT catalysts for fixed-bed reactors [11]. A weak cobalt support interaction in silica-supported catalysts promotes high cobalt reducibility but, on the other hand, favors agglomeration of supported cobalt particles. A solid-state reaction between silica and cobalt oxides could also result in mixed oxide (cobalt silicate) [12–16], which should be avoided, since it does not catalyze FT synthesis. Minimization of the concentration of barely reducible cobalt silicate and maximization of cobalt metal dispersion would therefore result in a better catalytic performance. Previous reports [17–19] have shown that cobalt metal dispersion in the final catalysts is usually affected by Co_3O_4 dispersion in the oxidized catalyst precursors.

Our earlier works [20–24] show that catalyst porosity seems to be one of the properties needed for the design of FT catalysts with a desired metal dispersion. It was found that in the catalysts prepared by impregnation with cobalt nitrate within a wide range of cobalt surface densities, cobalt dispersion was largely influenced by the porous structure of the support. Larger and easily reducible cobalt particles were detected in wider pore supports.

This paper focuses on the effect of cobalt precursor and the conditions of catalyst pretreatment on the structure of cobalt species and their catalytic performance in silica-supported FT catalysts prepared via impregnation with aqueous solutions of cobalt nitrate or acetate. At the different stages of their preparation (from aqueous impregnation through calcination and reduction), the catalysts were characterized by X-ray diffraction (XRD), UV–visible spectroscopy, X-ray photoelectron spectroscopy (XPS), X-ray absorption spectroscopy (XAS), DSC-TGA thermal analysis, propene chemisorption, and temperature-programmed reduction (TPR) combined with in situ magnetization measurements. The characterization results are discussed, together with the results of an evaluation of catalytic performance in FT synthesis with a fixed-bed microreactor.

2. Experimental

2.1. Catalyst preparation

Cobalt catalysts (Table 1) were prepared via incipient wetness impregnation with aqueous solutions of cobalt nitrate or cobalt acetate. Cab-osil M-5 fumed silica (S_{BET} = 214 m^2/g) was used as a catalytic support in all catalyst preparations. Before impregnation Cab-osil M5 was agglomerated by wetting and dried at 373 K. The concentrations of the impregnating solutions were calculated to obtain 10% cobalt in the final catalysts. After impregnation the catalysts were dried overnight in an oven at 363 K. Then they were calcined in airflow at temperatures ranging from 373 to 673 K. The catalysts were labeled CoAnionT, where Anion (N = nitrate or Ac = acetate) designates a cobalt salt used in the impregnation and T indicates the temperature of the oxidative pretreatment. After oxidative pretreatment the catalysts were reduced in a flow of hydrogen at 673 K for 5 h. The rates of temperature ramping during the oxidative treatment and reduction were 1 and 5 K/min, respectively. The cobalt content in the catalysts was measured by atomic absorption at the "Service Central d'Analyse du CNRS" (Vernaison, France). The specific surface areas and porosity of the oxidized catalysts were measured by low-temperature nitrogen adsorption with the use of the BET method (Table 1).

2.2. X-ray diffraction

X-ray powder diffraction patterns were recorded with a Siemens D5000 diffractometer and Cu(K_α) radiation. The average crystallite size of Co_3O_4 was calculated according to the Scherrer equation [25], with a (440) peak at 2θ = 65.344°.

Table 1
Characterization of cobalt silica supported catalysts

Catalyst	Cobalt content (wt%)	BET surface area (m^2/g)	Size of Co_3O_4 crystallites from XRD (nm)	$I_{Co_{2p}}/I_{Si_{2p}}$ ratio (XPS) in the oxidized samples[a]	Relative concentration of metallic cobalt in the reduced catalysts from XPS (%)	Propene chemisorption (μmol/g)
CoN373	9.85	128	< 9.6	2.22	20	17.4
CoN423	9.85	180	12.3	0.68	60	26.1
CoN673	9.85	185	20.0	0.33	65	22.1
CoAc443	9.52	163	–	2.45	26	12.9
CoAc493	9.52	–	–	2.0	–	7.5
CoAc673	9.52	162	–	1.63	11	1.2

[a] $I_{Co_{2p}}/I_{Si_{2p}}$ ratios were, respectively, 2.45 and 3.35 in the impregnated and dried catalysts prepared from cobalt nitrate and cobalt acetate.

2.3. UV–visible spectroscopy

Diffuse reflectance UV–visible spectra for catalysts and catalyst precursors were obtained under ambient conditions with a Varian-Cary 4 spectrophotometer, with $BaSO_4$ as a reference.

2.4. DSC-TGA

Simultaneous differential scanning calorimetry and thermogravimetric analysis were carried out in a flow of air at a heating rate of 1 K/min with a DSC-TGA SDT 2960 thermal analyzer. The sample loading was typically 10–15 mg.

2.5. X-ray absorption

X-ray absorption measurements were carried out at the 42 beamline in L.U.R.E., Orsay (France), with synchrotron radiation from the DCI storage ring running at 1.85 GeV, with an average current of 250 mA. The XAS data were taken at room temperature in air in the transmission mode through a Si (111) channel cut monochromator, with the use of two ionization chambers for X-ray detection. We calibrated the monochromator by setting the first inflection point of the K-edge spectrum of the Co foil at 7709 eV. The time required to measure an X-ray absorption spectrum (7600–8400 eV) was about 25 min.

XANES spectra obtained after background correction were normalized by the edge height. After cobalt atomic absorption was subtracted, the extracted EXAFS signal was transformed without phase correction from k space to r space (k^2, Hanning window) to obtain the radial distribution function (RDF).

Crystalline Co_3O_4, CoO, Co foil, and α- and β-cobalt silicate were used as standard compounds for XANES and EXAFS data analysis. Co_3O_4 has a spinel structure with Co^{2+} ions in tetrahedral coordination and Co^{3+} in octahedral coordination. CoO has a NaCl-type structure in which all Co atoms are situated in an octahedral environment. Three polyforms of Co_2SiO_4 are known [28]; in all of them Co atoms are located in a distorted octahedral environment. The α-form has an olivine (orthorhombic) type structure with the following average coordination distances for the first three shells: 6 CoO, 2.07 to 2.23 Å; 1.5 Co–Si, 2.72 to 2.81 Å; and 3 Co–Co, 3.0 to 3.22 Å. More information about the coordination of cobalt in Co_3O_4, CoO, and α-cobalt silicate is available from previous reports [24,26,27]. The β and γ forms of cobalt silicate [28] represent spinel-like (wadsleyite) and spinel structures, respectively, with average coordination distances for the first three shells of 2.05–2.15 Å (6 Co–O), 2.88 to 3.09 Å (6–6.5 Co–Co), and 3.28 to 3.40 Å (5.2–6 Co–Si) [15]. The XANES spectra and moduli of the Fourier transform of EXAFS of the reference compounds are presented in Figs. 1a and 1b. The good crystallinity of all reference samples was previously confirmed by XRD [15,27].

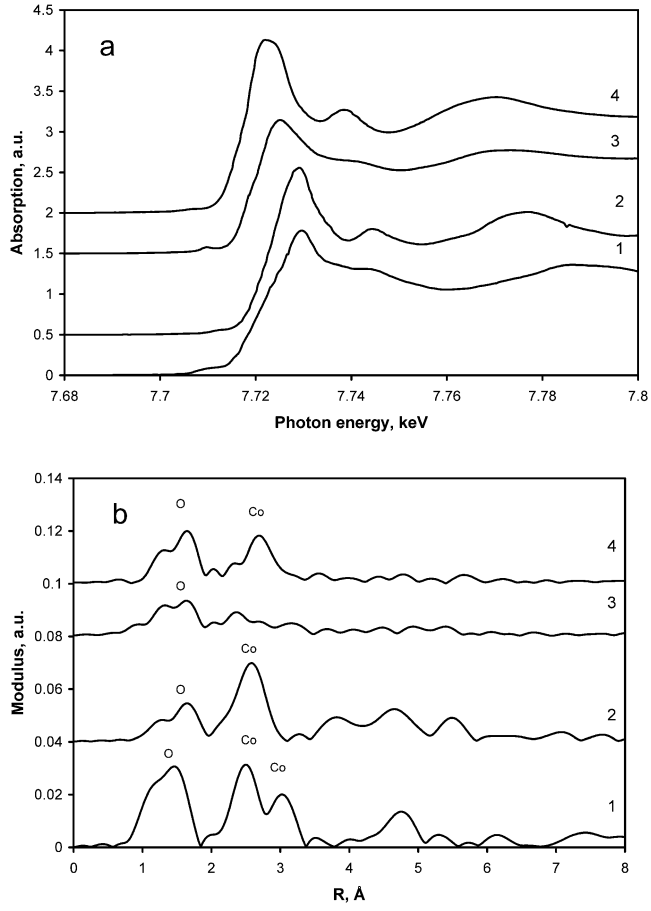

Fig. 1. XANES spectra (a) and moduli of Fourier transform of EXAFS (b) of the reference compounds: Co_3O_4 (1), CoO (2), α- (3) and β-cobalt silicate (4).

2.6. XPS

Surface analyses were performed with a VG ESCALAB 220XL spectrometer. The Al-K_α nonmonochromatized line (1486.6 eV) was used for excitation with 300-W of applied power. The analyzer was operated in a constant pass energy mode ($E_{pass} = 40$ eV). Binding energies were referenced to the Si 2p core level (103.6 eV) of the SiO_2 support. The reproducibility was ± 0.2 eV for Co 2p binding energy. The vacuum level during the experiment was better than 10^{-7} Pa. The powdered catalyst was pressed as a thin pellet onto a steel block. In situ reduction was carried out in pure hydrogen at 673 K for 5 h in the reactor cell of the preparation chamber attached to the analysis chamber of the spectrometer. Then the reduced sample was transferred to the analysis chamber of the spectrometer; the preparation and analysis chamber were linked hermetically. The sample was transferred from the preparation to the analysis chamber under vacuum without exposure to air.

The experimental Co 2p XPS spectra of the catalysts were normalized by the intensity of Si 2p line. To avoid any calibration problems due to the XPS spectrometer, the $2p_{1/2}$ $2p_{3/2}$ spin-orbital splittings and intensity of satellite structures were used in addition to the absolute Co 2p binding

energies, for the analysis of XPS data. The particle sizes of Co species in the oxidized and reduced catalysts were estimated with the Kerkhof–Moulijn model [23,29].

2.7. Combined in situ magnetic measurements and TPR

We made in situ magnetization measurements and obtained temperature-programmed reduction profiles by passing 5% H_2/Ar gas mixture through the catalyst while increasing the temperature at a linear rate. The experiments were carried out in the reactor, which was simultaneously a vibrating magnetometer cell [30]. This setup allows in situ monitoring of sample magnetization during standard temperature-programmed experiments. All quantitative information about the concentration of the cobalt metal phase was extracted from magnetic measurements. The TPR curves were used only for the qualitative analysis of cobalt reducibility; they were normalized to unity.

The amount of samples for all experiments was about 30 mg. The gas flow velocity was 30 ml/min; the rate of temperature ramping was 12 K/min. These conditions were used to satisfy the commonly used TPR criteria [31]. The reduction gas mixture was purified with the use of water and oxygen traps.

Because of the high Curie temperature of Co, the magnetization of the sample is proportional to the amount of the metallic cobalt in the sample up to 673–773 K [32,33]. At higher temperatures the data were corrected by a standard procedure based on the dependence of saturation magnetization on temperature. The amount of reduced cobalt was estimated by approximation magnetization-field dependence of the sample at room temperature to the infinity field.

2.8. Propene chemisorption

The number of surface metal sites in the catalysts was evaluated by propene chemisorption in a pulse reactor. After reduction in pure hydrogen at 673 K for 5 h, the catalyst (0.1 g) was cooled and purged with He at 323 K. Pulses of propene (0.1 ml) were introduced into the flow of He. The relative number of metal surface sites was estimated from the amount of chemisorbed propene. No propene chemisorption was observed on pure silica support. This method provides only relative information about the concentration of cobalt metal sites. Note that no assumption was made about the stoichiometry of propene chemisorption or about the absolute number of cobalt metal sites in the reduced cobalt catalysts.

Analysis of the reaction products was performed using gas chromatography with a Chrompack PLOT (KCl/Al_2O_3) semi-capillary column. The pulse experiments were completed, when the detector showed no propene chemisorption.

2.9. Catalytic measurements

Carbon monoxide hydrogenation was carried out in a fixed-bed stainless-steel tubular microreactor ($d_{int} = 9$ mm) operating at 463 K under atmospheric pressure. The thermocouple was in direct contact with the catalyst. The reaction design permitted measurement of the temperature along the catalyst bed; no heat spot was detected in the catalyst bed during the FT reaction. Carbon monoxide conversion was lower than 10% in all experiments.

The catalyst was crushed and sieved to obtain catalyst grains 0.05–0.2 mm in diameter. The catalyst loading was typically 0.5 g. The samples were reduced in hydrogen flow at 673 K for 5 h. After the reduction, a flow of premixed synthesis gas with a H_2/CO molar ratio of 2 was passed over the catalysts. The carbon monoxide contained 5% nitrogen, which was used as an internal standard for calculating carbon monoxide conversion. To avoid possible condensation of the reaction products, the gas transfer lines were constantly heated. Gaseous reaction products were analyzed on-line by gas chromatography. Analysis of H_2, CO, CO_2, and CH_4 was performed with a 13X molecular sieve column and a thermal conductivity detector. Hydrocarbons (C_1–C_{18}) were separated in 10% CP-Sil5 on a Chromosorb WHP packed column and analyzed with a flame-ionization detector. Analysis of lighter paraffins and olefins (C_1–C_7) was carried out with an HP-PONA capillary column. The hydrocarbon selectivities were calculated on a carbon basis. The Anderson–Schulz–Flory (ASF) chain growth probabilities were calculated from the slope of the curve $\ln(S_n/n)$ versus n, where n is the carbon number and S_n is the selectivity for the C_n hydrocarbon. The chain growth probability was calculated for the C_4–C_{16} hydrocarbon range. The FT reaction rate is expressed as cobalt-time yield (in moles of converted CO per second divided by the total amount of cobalt (in moles) loaded into the reactor).

3. Results

3.1. Impregnated and dried catalysts

UV–visible spectra for cobalt nitrate and cobalt acetate impregnation solutions are shown in Figs. 2a and 2b. They both exhibit a broad band at 510 nm, which, in agreement with previous reports [34–36], was assigned to the $^4T_{1g}(F) \rightarrow {}^4T_{1g}(P)$ transition in octahedral high-spin Co^{2+} complexes. The broad band at 510 nm remains intense in the impregnated and dried samples. This suggests that cobalt keeps predominantly an octahedral coordination after deposition from cobalt acetate or cobalt nitrate solutions on the silica surface. In addition, a weak band of absorption at 730 nm is observed in the spectra of dried samples (Fig. 2a, curve 2), which might be due [35,37] to the presence of a low-concentration Co_3O_4 phase generated by cobalt nitrate hydrolysis. The UV–visible data are in good agreement with X-ray absorption measurements. The XANES spectra for the catalysts prepared from both cobalt nitrate and acetate are similar to the spectra for the corresponding salts (Figs. 3 and 4). In both cobalt nitrate and cobalt acetate salts and in the catalysts after impregnation and drying, the

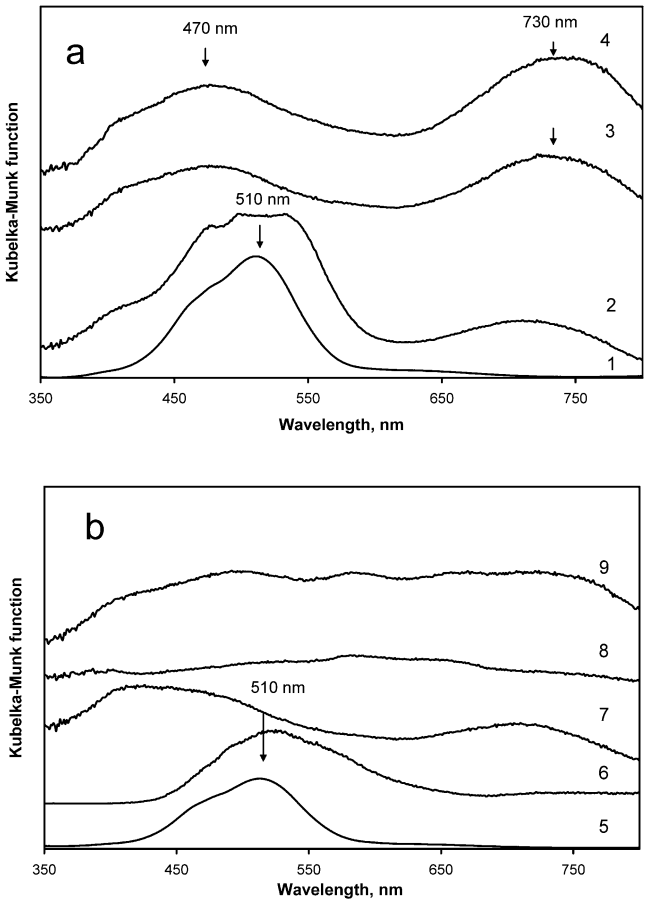

Fig. 2. UV–visible spectra of cobalt precursors and silica catalysts prepared using impregnation with cobalt nitrate (a) and cobalt acetate (b): impregnating cobalt nitrate solution (1), silica after impregnation with cobalt nitrate and drying (2), CoN373 (3), CoN673 (4), impregnating cobalt acetate solution (5), silica after impregnation with cobalt acetate and drying (6), CoAc443 (7), CoAc493 (8), and CoAc673 (9).

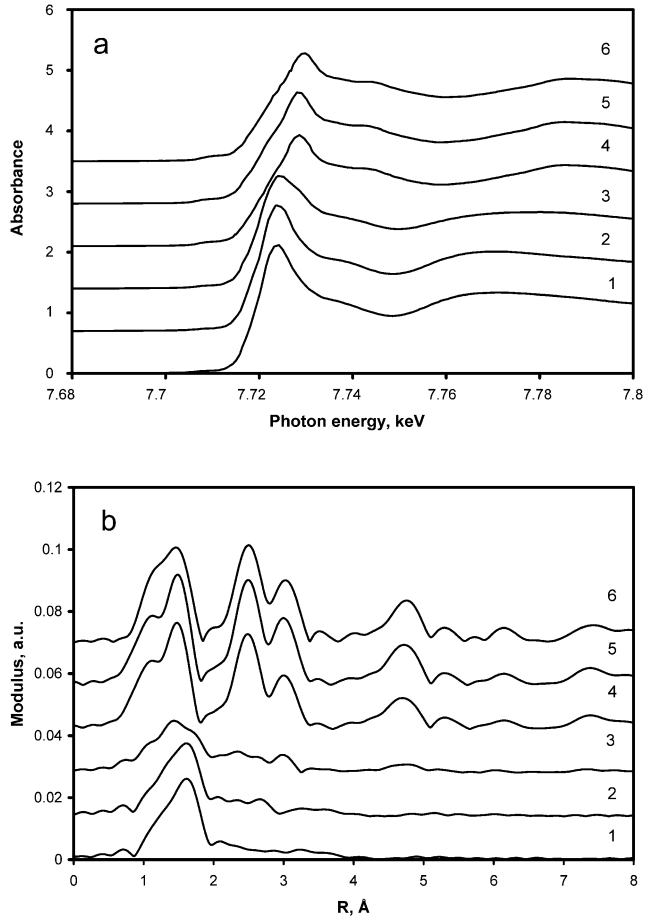

Fig. 3. XANES spectra (a) and moduli of Fourier transform of EXAFS (b) of calcined silica supported catalysts prepared using impregnation with cobalt nitrate: bulk cobalt nitrate (1), silica after impregnation with cobalt nitrate and drying (2), CoN373 (3), CoN423 (4), CoN673 (5), and bulk Co_3O_4 (6).

Fourier transform moduli of EXAFS exhibit an intense peak at 1.62–1.65 Å, which is probably due an oxygen octahedral environment of cobalt atoms. The X-ray absorption data suggest, therefore, that in the first coordination shell cobalt atoms are probably surrounded by six oxygen atoms.

Co 2p XPS data are shown in Fig. 5. They are also consistent with the results obtained by UV–visible and X-ray absorption spectroscopies. The intense satellite structure [38,39] and high energy of the XPS Co $2p_{3/2}$ peaks (782.6 eV) indicate the presence of Co^{2+} ions in the impregnated and dried catalysts prepared from cobalt acetate or nitrate.

Thus the characterization results suggest that after deposition on silica and drying, cobalt is present mostly as Co^{2+} ions at the octahedral coordination close to that in the impregnating cobalt nitrate and acetate solutions.

3.2. Oxidative pretreatment of catalyst precursors

3.2.1. Decomposition of cobalt nitrate and cobalt acetate

Fig. 6 presents curves for DSC-TGA in air for the catalysts prepared from cobalt acetate and cobalt nitrate. The weight loss and heat flow curves exhibit several inflections at 323–473 K, which are probably due to the endothermic loss of water molecules in the cobalt hydrate shell and to the decomposition of the nitrate or acetate anions. The heat flow curves show that decomposition of cobalt nitrate was endothermic, whereas decomposition of cobalt acetate was highly exothermic. Decomposition of supported cobalt nitrate occurs at 423 K (Fig. 6a). Decomposition of supported cobalt acetate proceeds at slightly higher temperatures (Fig. 6b); the principal heat flow peak is located at 493 K.

Co_3O_4 is the product of decomposition of both pure cobalt nitrate and cobalt acetate salts in air (DSC-TGA curves not shown). Previous reports [40] showed that the decomposition of cobalt nitrate proceeds with the release of nitrogen dioxide, water, and oxygen:

$$3Co(NO_3)_2 \cdot 6H_2O \rightarrow Co_3O_4 + 6NO_2 + O_2 + 18H_2O.$$

Like the profile of the catalysts prepared from cobalt acetate, the TGA profile of the pure cobalt acetate salt exhibits a weight loss at 323–423 K, probably because of the loss of hydrate water molecules. The DSC curve shows an exothermic peak at 517–520 K. In agreement with previous data

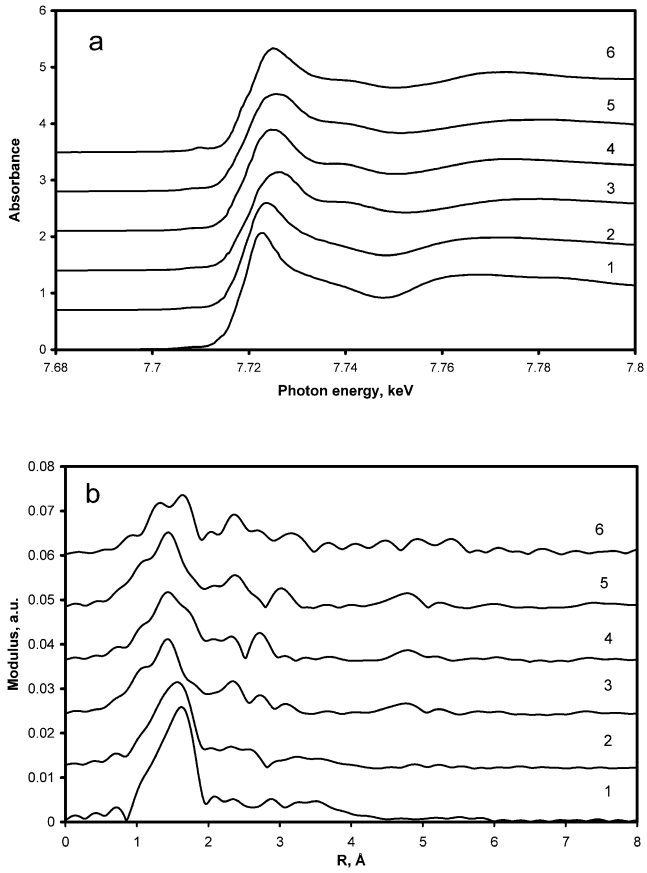

Fig. 4. XANES spectra (a) and moduli of Fourier transform of EXAFS (b) of calcined silica supported catalysts prepared using impregnation with cobalt acetate: bulk cobalt acetate (1), silica after impregnation with cobalt acetate and drying (2), CoAc443 (3), CoAc493 (4), CoAc673 (5), and α-cobalt silicate (6).

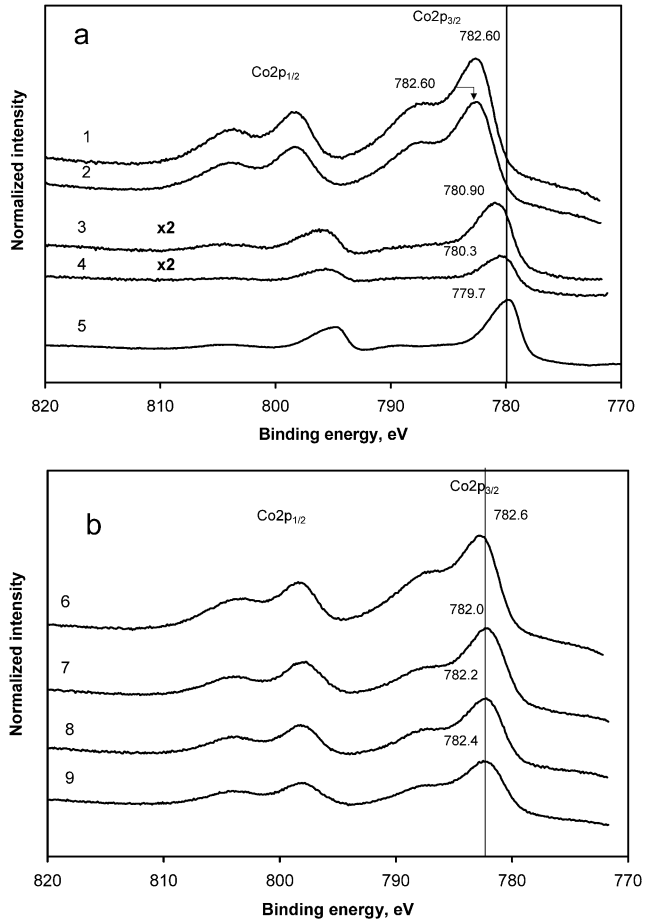

Fig. 5. Co 2p XPS spectra of calcined catalysts prepared using impregnation with cobalt nitrate (a) and cobalt acetate (b): silica after impregnation with cobalt nitrate and drying (1), CoN373 (2), CoN423 (3), CoN673 (4), reference Co_3O_4 sample (5), silica after impregnation with cobalt acetate and drying (6), CoAc443 (7), CoAc493 (8), and CoAc673 (9). The XPS spectra are normalized by the intensity of Si 2p line and offset for clarity.

[41,42], the observed exothermic peak could be attributed to acetate combustion, which leads to the release of carbon dioxide and water:

$$3Co(CH_3COO)_2 \cdot 4H_2O + 12.5O_2 \rightarrow Co_3O_4 + 12CO_2 + 21H_2O.$$

As was shown earlier [41], the strong exothermic effect is caused by an autocatalytic oxidation due to the generation of cobalt oxide during cobalt acetate decomposition.

The scarcity of information about the extent of hydration of supported cobalt ions makes it difficult to evaluate the stoichiometry of decomposition of cobalt nitrate and cobalt acetate in the impregnated and dried catalyst precursors. The estimations show, however, that some of the water molecules from the cobalt hydrate shell have already been lost during drying of the impregnated samples in an oven; the weight losses of both silica-supported cobalt nitrate (experimental weight loss 16%) and acetate (experimental weight loss 12%) were considerably lower (Figs. 6a and 6b) than those that could be expected from the decomposition of fully hydrated $Co(NO_3)_2 \cdot 6H_2O$ (theoretic weight loss 29.4%) and $Co(CH_3COO)_2 \cdot 4H_2O$ (theoretic weight loss 24.7%) complexes.

3.2.2. Cobalt species in oxidized CoN catalysts

The structure of cobalt species in the catalysts prepared from cobalt nitrate and cobalt acetate, which were calcined at different temperatures, was characterized by UV–visible spectroscopy, XRD, XAS, and XPS.

In all calcined catalysts prepared from cobalt nitrate, XRD reveals the presence of a Co_3O_4 crystalline phase (Fig. 7). Much broader XRD peaks indicate smaller Co_3O_4 crystallite sizes in the samples calcined at lower temperature (CoN373, CoN423). The diameters of Co_3O_4 crystallites calculated from the width of the (440) diffraction peak are shown in Table 1. The diameter of Co_3O_4 crystallites increases with an increase in the calcination temperature from 373 to 673 K.

The near-edge X-ray absorption spectrum of CoN373 resembles that of the bulk cobalt nitrate (Fig. 3a). This suggests a similar local coordination of cobalt in CoN373 and in bulk cobalt salt. The Fourier transform modulus (Fig. 3b) was different, however, from that of bulk cobalt nitrate. It presents a broad peak at 1.45–1.7 Å, which is likely to be at-

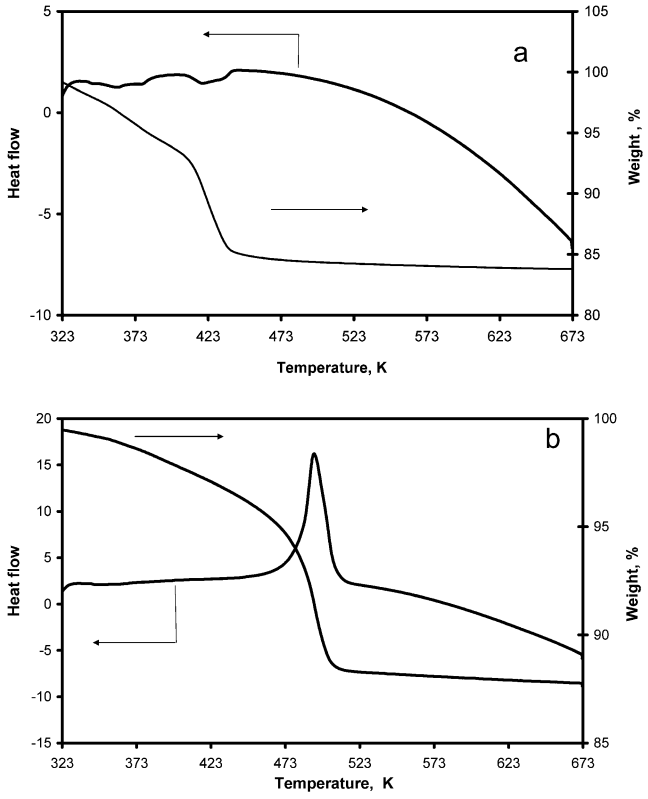

Fig. 6. DSC-TGA curves of silica supported cobalt nitrate (a) and acetate (b). Temperature ramp 1 K/min.

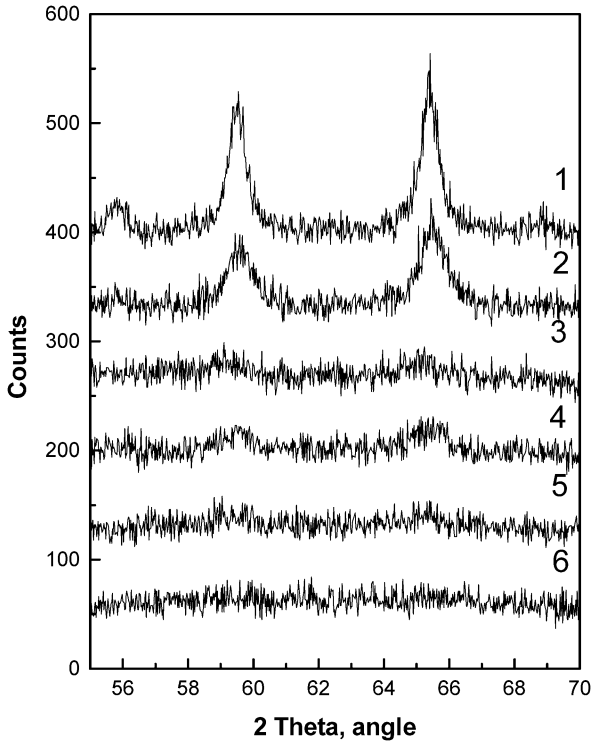

Fig. 7. XRD patterns of oxidized cobalt catalysts prepared from cobalt nitrate or cobalt acetate: CoN673 (1), CoN423 (2), CoN373 (3), CoAc673 (4), CoAc493 (5), and CoAc443 (6). The XRD patterns are offset for clarity.

tributed to several CoO coordination shells. The large width of the peak probably suggests the presence of a mixture of cobalt oxides and nitrates in the CoN373 catalyst and agrees well with UV–visible data.

Oxidative pretreatment at temperatures higher than 373 K results in significant modifications of X-ray absorption spectra. Fig. 3a shows that the XANES spectra of CoN423 and CoN673 are almost identical to that of Co_3O_4. The moduli of the Fourier transform (Fig. 3b) consist of several peaks characteristic of the Co_3O_4 structure. Co_3O_4 has a spinel structure with Co^{2+} ions occupying tetrahedral sites and Co^{3+} occupying octahedral sites [26]. In agreement with previous reports, the broad peak at 1.47 Å is attributed to CoO coordination for both Co^{2+} and Co^{3+} coordination shells. These two coordination shells are usually not resolved in Fourier transform moduli [24,27]. The overlapped peaks at 2.50 and 3.02 Å are attributed to CoCo coordinations in Co_3O_4. More detailed information about attribution of the peaks in the modulus of the Fourier transform of EXAFS of Co_3O_4 is available in our previous publications [15,24,27]. Thus, in agreement with DSC-TGA results, XANES and EXAFS data strongly suggest that cobalt nitrate supported on silica decomposes in air at 373–423 K. Co_3O_4 appears to be the predominant cobalt phase in both CoN423 and CoN673 catalysts.

Co 2p XPS spectra for CoN423 and CoN673 are very similar to the spectrum for the reference Co_3O_4 sample (Fig. 5a). In agreement with previous reports [39,43–47], the Co_3O_4 Co $2p_{3/2}$ binding energies were about 780 eV; the spin-orbital splittings were 15.1 eV. The spectra of both CoN423 and CoN673 and the reference Co_3O_4 show only very weak shake-up satellites centered at approximately 789.5 and 804.5 eV, about 10 eV from the main bands, as reported earlier [39]. This observation is consistent with X-ray absorption data (XANES, EXAFS), which suggest the presence of significant Co_3O_4 concentrations in the catalysts calcined at temperatures higher than 373 K. The $I_{Co_{2p}}/I_{Si_{2p}}$ ratio measured from XPS data was lower after calcination at 673 K than at 423 K (Table 1). This suggests the presence of larger Co_3O_4 particles in CoN673. The sizes of Co_3O_4 particles calculated for CoN673 and CoN423 with the use of the Kerkhof–Moulijn model [23,29] were 16.8 and 7.5 nm, respectively, which is consistent with the XRD crystallite size evaluation made with the Scherrer equation (Table 1). For the catalyst pretreated at 373 K (CoN373), the higher energy of the Co 2p XPS line (782.6 eV) and the intense satellite structure confirmed the presence of Co^{2+} ions, which were also detected by X-ray absorption spectroscopy.

UV–visible spectra for calcined CoN373 and CoN673 are presented in Fig. 2a. They exhibit two broad bands at 730 and 470 nm. In agreement with previous reports [35,37], these bands are related to Co_3O_4 species.

3.2.3. *Cobalt species in oxidized CoAc catalysts*

Oxidative treatment of the catalysts prepared from cobalt acetate leads to characterization data that are very different

from those obtained for the catalysts obtained from cobalt nitrate. Only very low, intense Co_3O_4 diffraction peaks were detected in the catalysts prepared from cobalt acetate (Fig. 7). This suggests a very low concentration of the Co_3O_4 crystalline phase.

X-ray absorption data for the catalysts prepared from cobalt acetate are shown in Fig. 4. The XANES and particularly EXAFS are very different for Co_3O_4 and the catalysts prepared from cobalt nitrate. The X-ray absorption data were compared with those for reference cobalt silicate compounds and were found to be rather similar to those for α-Co_2SiO_4 with an orthorhombic olivine-type structure. The XANES spectra for calcined CoAc catalysts and α-Co_2SiO_4 were almost identical (Fig. 4a). The moduli of the Fourier transform of EXAFS (Fig. 4b) are constituted by a set of peaks attributed to CoO, CoSi, and CoCo distances similar to those in the silicate olivine structure [15]. Similar XANES spectra and Fourier transform moduli suggest a similar cobalt coordination in CoAc samples in α-Co_2SiO_4. It can be suggested, therefore, that during decomposition of cobalt acetate, cobalt ions react with silica, yielding structures similar to that of orthorhombic α-cobalt silicate.

Fig. 5b presents XPS data for the calcined CoAc samples. They exhibit an intense satellite structure centered at 797 and 804 eV characteristic of Co^{2+} ions [39,48,49]; the orbital splitting was 15.7 eV. The main Co $2p_{3/2}$ peak shifts to higher binding energies (782–782.4 eV) relative to the spectrum of the reference Co_3O_4 sample (Fig. 5). It is clear that the electronic structure of cobalt species present in the calcined catalyst prepared from cobalt acetate is very different from that of Co_3O_4. Note that the XANES spectrum and EXAFS modulus (Fig. 4) were also very different from those of the reference Co_3O_4 and CoO. This suggests that no noticeable concentration of Co_3O_4 or CoO is present in any catalyst prepared from cobalt acetate. This finding seems to be in line with a high concentration of amorphous cobalt silicate in the catalyst precursors prepared from cobalt acetate predicted by XRD and discovered by X-ray absorption. The $I_{Co_{2p}}/I_{Si_{2p}}$ ratio measured by XPS decreases with the calcination temperature (Table 1). This suggests migration of Co^{2+} ions from the external surface to the interior of silica as the calcination temperature increases.

UV–visible spectra for CoAc catalysts at 443–673 K are shown in Fig. 2b. Oxidative pretreatment of the catalyst prepared from cobalt acetate at relatively low temperature (443 K) leads to the appearance of two broad bands at 450 and 730 nm that are characteristic of Co_3O_4 [35,37]. This suggests the presence of Co_3O_4 particles in the catalysts obtained via soft decomposition of cobalt acetate. Decomposition of cobalt acetate at temperatures higher than 443 K does not produce any bands typical of Co_3O_4.

3.3. Co species in the reduced catalysts

Reduction of cobalt species in CoN and CoAc samples was followed by TPR combined with in situ magnetic measurements. Figs. 8 and 9 show that the TPR profiles for both CoN and CoAc catalyst series are rather complex. They comprise several overlapping peaks, which are probably due to the reduction of supported cobalt oxide species. In the catalysts precalcined at lower temperatures, some TPR peaks might also be assigned to the decomposition in the presence of hydrogen of residual cobalt nitrate and acetate species.

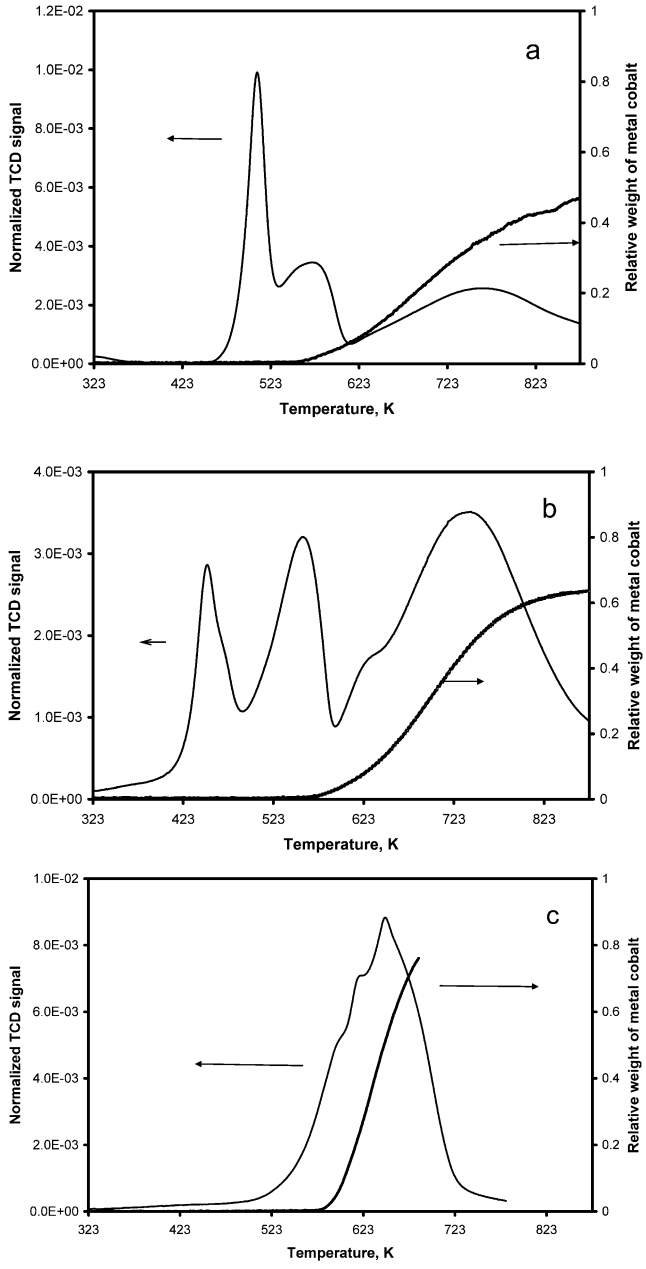

Fig. 8. TPR profiles and magnetization curves of cobalt catalysts prepared from cobalt nitrate: CoN373 (a), CoN423 (b), and CoN673 (c) (temperature ramp 12 K/min).

Calcination temperature has a significant effect on the peak maxima. A lower temperature of decomposition of cobalt precursor generally leads to the shift of TPR peaks to lower temperatures. This finding is in agreement with the report by van Steen et al. [14], who found that low-temperature

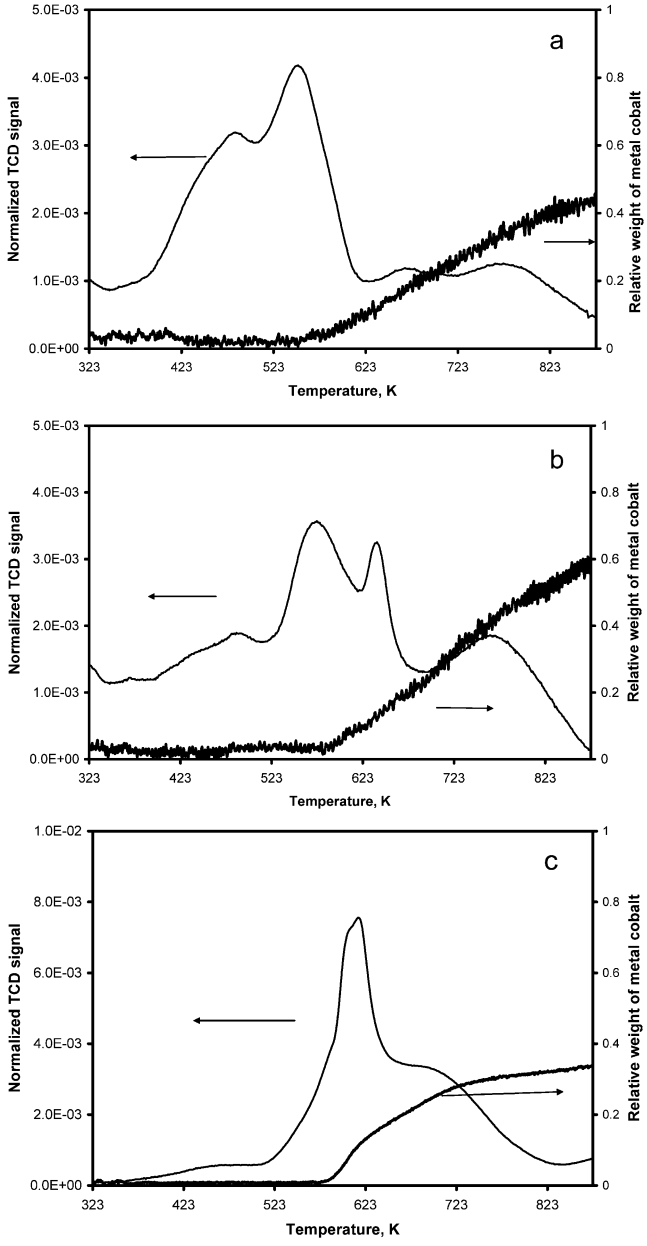

Fig. 9. TPR profiles and magnetization curves of cobalt catalysts prepared from cobalt acetate: CoAc443 (a), CoAc493 (b), and CoAc673 (c) (temperature ramp 12 K/min).

calcination (473–523 K) of cobalt silica-supported catalysts resulted in a higher intensity of low-temperature hydrogen consumption peaks in TPR profiles. In the paper by van Steen et al. [14] some of these peaks were attributed to the reductive decomposition of residual nitrate ions. In our work the catalysts were precalcined at temperatures lower than they were in the study by van Steen. Thus it seems even more probable that some of the lower temperature TPR peaks (Figs. 8 and 9) could be related to reductive decomposition of nitrate or acetate species.

In situ magnetization measurements appear to be particularly helpful in the interpretation of complex TPR profiles. Figs. 8 and 9 show that most low-temperature TPR peaks are not associated with an increase in magnetization. This suggests that those low-temperature TPR peaks are not associated with the release of any cobalt metal phase; they are probably due either to the partial reduction of Co_3O_4 to CoO or to the decomposition of the residual cobalt precursors. This indicates that no cobalt metal phase is produced below 573 K on cobalt silica-supported catalysts prepared from cobalt acetate or nitrate. On both CoAc and CoN series, the cobalt metal phase occurs at temperatures above 573 K. Its concentration depends on both the initial cobalt salt (nitrate or acetate) and the temperature of oxidative pretreatment.

A higher magnetization and thus a higher concentration of cobalt metal phase were observed in the CoN673 catalyst, which was prepared from cobalt nitrate and was precalcined at relatively high temperature (673 K). This is consistent with the dependence of cobalt dispersion in this catalyst on the calcination temperature and with the presence of larger cobalt oxide particles detected by XRD. Previous reports [18,27,50,51] showed that larger cobalt oxide particles supported on silica could be reduced much more easily than smaller ones. A much lower concentration of cobalt metal phase detected in CoAc samples (Fig. 9) is likely to be related to the presence of larger concentrations of amorphous, barely reducible cobalt silicate.

Additional information about the concentration of cobalt metal species in the reduced samples is available from XPS experiments. XPS spectra for the catalysts reduced at 673 K in pure hydrogen are shown in Fig. 10. Cobalt metal phase was identified in the XPS spectra by Co 2p binding energies (Co $2p_{3/2} = 778$ eV), spin-orbital splitting (15.0 eV), and line shape [18,52]. The XPS spectra were simulated with the use of Eclipse software provided by ThermoVG Scientific. Shirley background subtraction and alignment of binding energy were carried out for the experimental XPS spectra. Two sets of linked parameters were used for the simulation of XPS spectra. The sets of linked parameters for Co^{2+} and Co metallic species (energy center separation, width and height ratio, Gaussian/Lorentzian form, asymmetry) were determined from the XPS spectrum of Co^{2+} ions in the oxidized 10CoAc673 sample and Co^0 species in the reference Co metal spectrum [53]. The relative amount of Co metal phase (Table 1) was estimated from a fit of the experimental and simulated XPS profiles.

XPS data confirm the effect of temperature of oxidative pretreatment on cobalt reducibility observed with the combined TPR and magnetic method. Primarily cobalt metallic species were detected in the reduced CoN673 and CoN423 samples. The Kerkhof–Moulijn model provides the following sizes for cobalt metal particles: 7.2 nm (CoN423) and 8.4 nm (CoN673). A much lower relative concentration of cobalt metal phase was observed in CoN373 catalysts. One of the reasons for the lower extent of cobalt reduction in CoN373 could be the presence of small Co_3O_4 crystallites, which are less reducible in hydrogen.

Less cobalt reduction was found by XPS in the catalysts prepared from cobalt acetate (Fig. 10b, Table 1). This obser-

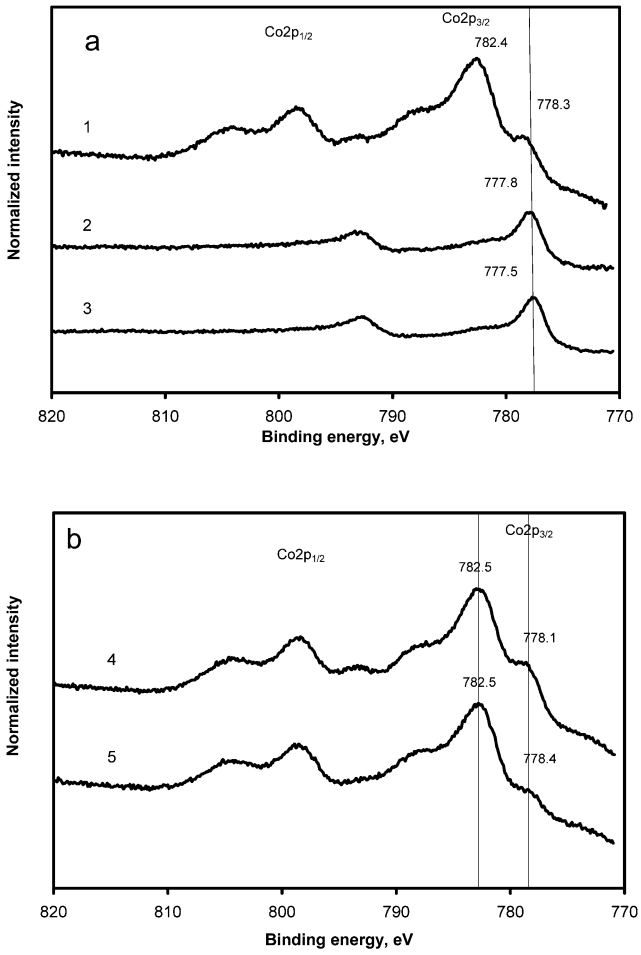

Fig. 10. Co 2p XPS spectra of catalysts prepared using impregnation with cobalt nitrate (a) and cobalt acetate (b) reduced in pure hydrogen at 673 K: CoN373 (1), CoN423 (2), CoN673 (3), CoAc443 (4), and CoAc673 (5). The XPS spectra are normalized by the intensity of Si 2p line and offset for clarity.

vation is consistent with the TPR-magnetic data and is probably due to the presence of a considerable concentration of amorphous, barely reducible cobalt silicate. Fig. 10b shows, however, that the relative intensities of the Co $2p_{3/2}$ XPS lines at 777–778 eV attributed to metallic cobalt were higher with the CoAc443 catalyst prepared from acetate, which was precalcined at lower temperatures (Fig. 10b, curve 4). The more quantitative data are displayed in Table 1.

Note that somewhat lower concentrations of cobalt metal phase were measured by the magnetic method relative to XPS, though the trends in the evolution of cobalt reducibility observed with the two techniques were similar. It should be taken into consideration that TPR combined with magnetic measurement was carried out with diluted hydrogen (5% H_2/Ar), whereas the catalysts were reduced in pure hydrogen before XPS analysis. Therefore, a lower concentration of cobalt metal phase in CoN423 and CoAc samples measured by the magnetic method relative to XPS is likely to be attributed to the lower partial pressure of hydrogen in the TPR measurements. Examination of the results obtained by both techniques (Figs. 8–10, Table 1) suggests the following qualitative order of decreasing cobalt reducibility in the investigated catalysts: CoN673 > CoN423 > CoN373, CoAc443 > CoAc493 > CoAc673.

Table 2
Catalytic performance of cobalt silica supported catalysts in FT synthesis

Catalyst	FT reaction rate (10^{-4} s^{-1})	S_{CH_4} (%)	$S_{C_{5+}}$ (%)	Alpha
CoN373	3.3	15	67	0.80
CoN423	3.7	18	62	0.85
CoN673	2.9	13	70	0.78
CoAc443	0.7	18	60	0.73
CoAc493	0.02	17	62	0.74
CoAc673	0.01	16	70	0.76

The relative number of cobalt surface metal sites in the reduced catalysts was measured by propene chemisorption (Table 1). The method confirms a higher concentration of cobalt metal sites in the catalysts prepared from cobalt nitrate, which generally undergo more cobalt reduction. The concentration of cobalt metal sites was higher in CoN423 than in the catalysts precalcined at lower and higher temperatures (CoN373 and CoN673). It is known that the number of cobalt metal sites depends on both cobalt dispersion and reducibility. A higher concentration of cobalt metal sites measured in CoN423 could therefore be attributed to a combination of high cobalt dispersion and good cobalt reducibility.

Table 1 also demonstrates that CoAc443 catalyst contains a higher concentration of cobalt metal sites than other catalysts prepared from cobalt acetate. This is consistent with XPS results, which show a higher relative concentration of cobalt metal phase in the CoAc443 sample (Fig. 10b). Better reducibility of CoAc443 could be assigned to the presence of Co_3O_4 phase, which was also identified in this catalyst by UV–visible spectroscopy (see Section 3.2).

3.4. Catalytic performance of CoN and CoAc catalysts in FT synthesis

The evaluation of catalytic performance was carried out in a differential catalytic reactor at 463 K; the carbon monoxide conversion was lower than 10%. Conversion of carbon monoxide and hydrogen over CoN and CoAc catalysts leads to a wide range of hydrocarbons and water. The catalytic activity decreased slowly during the first hours before attaining quasi-steady conditions after 5–6 h of reaction. The FT reaction rates and hydrocarbon selectivities were evaluated after 24 h on stream. We calculated the FT reaction rates (cobalt time yields) from carbon monoxide conversions and gas hourly space velocities; then we normalized the rates by the number of cobalt atoms loaded in the reactor. The catalytic activity data, together with selectivities for methane and light and heavier hydrocarbons are listed in Table 2.

The reaction rates and hydrocarbon selectivities for the catalysts prepared from cobalt nitrate were measured at car-

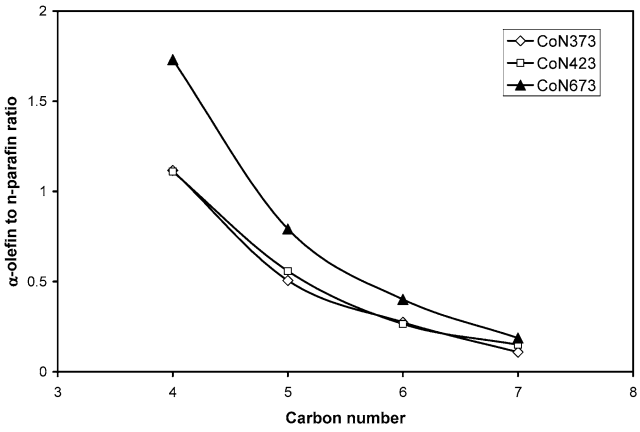

Fig. 11. α-Olefin to n-paraffin ratio over the catalysts prepared from cobalt nitrate at 7% carbon monoxide conversion.

bon monoxide conversions close to 7%. Table 2 shows that a lower temperature of calcination of CoN catalysts has only a slight effect on the FT reaction rate. The chain growth probability (α) was higher over the catalysts precalcined at lower temperatures (CoN373 and CoN423). These catalysts exhibited a slightly higher methane selectivity, however; $S_{C_{5+}}$ selectivity was around 62–70%. The ratios of α-olefin to n-parafin measured for C_4–C_7 hydrocarbons are presented in Fig. 11. Lower olefin concentrations were observed over CoN373 and CoN423 catalysts. In agreement with previous reports [7,54], the ratio decreases exponentially with carbon number. This suggests that the rate of olefin readsorption increases with the chain length.

Table 2 shows that the catalysts prepared from cobalt acetate were much less active in FT synthesis than those from cobalt nitrate. A lower temperature of oxidative pretreatment of the catalysts prepared from cobalt acetate leads, however, to a considerable increase in FT reaction rates. CoAc443 was more than 10 times more active than the catalysts obtained by cobalt acetate decomposition at higher temperatures (CoAc493 and CoAc673). Note that because of a much lower activity, hydrocarbon selectivities over the catalysts prepared from cobalt acetate were measured at significantly lower conversions (0.1–2%) than were the selectivities measured over the catalysts prepared from cobalt nitrate ($\sim$7%). This was why we made no direct comparison of hydrocarbon selectivities obtained over the catalysts prepared from cobalt nitrate or acetate.

4. Discussion

The results show that the nature of cobalt species in the silica-supported catalysts strongly depends on the type of cobalt precursor and catalyst pretreatment. Impregnation with cobalt nitrate and its subsequent decomposition lead to Co_3O_4. Impregnation with cobalt acetate results in a considerably lower concentration of crystalline Co_3O_4 phase in the oxidized catalysts and lower cobalt reducibility in hydrogen. Very low, intense peaks attributable to crystalline Co_3O_4 were observed by XRD for the catalysts prepared from cobalt acetate. Both XANES spectra and the moduli of the Fourier transform indicate local coordination of cobalt in CoAc samples close to that in orthorhombic α-cobalt silicate (Fig. 4). The suggestion that amorphous, barely reducible cobalt silicate is a dominant phase in the catalysts prepared from cobalt acetate is also consistent with earlier literature data [14,55].

In the previous work of van Steen et al. [14] the impregnation procedure was described by the concept of interfacial coordination chemistry; a higher concentration of cobalt silicate discovered after impregnation and calcination of cobalt acetate was attributed to higher pH of the impregnating acetate solution (pH 6–7). It was also suggested that a higher pH of the impregnation solution could lead to a partial dissociation of silanol groups. Thus, more cobalt complexes can interact with dissociated silanol groups, and this interaction would lead to a higher concentration of cobalt silicate. Ming et al. [56] showed that the pH of the impregnating solution influences the impregnation of silica with cobalt ions. For silica, the pH value, defined as the point of zero charge, is situated between 2 and 3.5. Below the pH of the point of zero charge, the surface of silica is positively charged and the adsorption of positively charged cobalt ions is slowed down. This would lead to the catalysts with lower cobalt dispersion. At pH higher than the point of zero charge, deposition of cobalt is favored, which should improve cobalt dispersion. At pH $>$ 5, silica gel partially dissolves. This may result in the direct substitution of silicon atoms by cobalt ions at the surface of silica.

The suggestion that a higher pH of cobalt acetate solution leads to the formation of cobalt silicate immediately after impregnation is not confirmed by our experimental data, however. Indeed, XANES spectra and the moduli of the Fourier transform of bulk cobalt acetate and cobalt acetate deposited on the silica surface via impregnation are almost identical (Fig. 4, curves 1 and 2). UV–visible spectroscopy shows that most cobalt atoms still maintain a octahedral coordination similar to those in cobalt acetate solution after impregnation and drying (Fig. 2b). This assumes a similar cobalt local coordination in cobalt acetate and impregnated catalysts.

It is more likely that cobalt silicate arises not from impregnation of silica with aqueous solutions of cobalt silicate but from the exothermal decomposition of supported cobalt acetate complexes during catalyst oxidative pretreatment. Indeed, characterization results indicate significant structural changes that occur during catalyst calcination. XANES spectra and Fourier transform moduli of EXAFS shift from those of cobalt acetate to the shapes rather similar to that of α-cobalt silicate (Fig. 4). The temperature of decomposition of supported cobalt acetate complexes seems to produce a pronounced effect on cobalt repartition between barely reducible cobalt silicate and easily reducible cobalt species. Some concentration of reducible Co_3O_4 was observed when catalyst pretreatment was carried out at lower temperatures

(CoAc443), whereas no Co_3O_4 was detected when acetate decomposition was carried out at higher temperatures. Thus, a lower cobalt silicate concentration after the decomposition of cobalt acetate at lower temperatures could be attributed to a better control of heat flow. This conclusion seems to be in agreement with the results of van Steen et al. [14], who showed that the occurrence of cobalt silicate in cobalt silica-supported catalysts can be avoided with a low-temperature drying process. It was suggested in that work [14] that drying or low-temperature calcination destroys the precursor of the cobalt silicate.

The temperature of cobalt acetate decomposition also affects the repartition of Co^{2+} ions between the external surface of silica and the silica volume. The lower $I_{Co_{2p}}/I_{Si_{2p}}$ ratio detected by XPS for the catalysts prepared from cobalt acetate and calcined at higher temperatures (Table 1) suggests that a solid-state reaction between cobalt oxide and silica at higher temperatures could lead to the migration of Co^{2+} ions to the silica core.

Co_3O_4 seems to be the dominant phase produced by the decomposition of supported cobalt nitrate. The presence of Co_3O_4 in all CoN samples after calcination was confirmed by XRD, XPS, and XANES/EXAFS. The concentration of Co_3O_4 seems to be much lower in the cobalt catalysts calcined at 373 K; a considerable concentration of cobalt ions still exists in a coordination similar to that of cobalt nitrate. XRD shows that cobalt dispersion in the catalysts prepared from cobalt nitrate appears to be a function of calcination temperature; the size of cobalt oxide crystallites measured with the Scherrer equation increases from 9 to 20 nm (Fig. 7 and Table 1). This observation is consistent with a lower XPS $I_{Co_{2p}}/I_{Si_{2p}}$ ratio observed in the CoN673 catalyst (Table 1). Low cobalt dispersion in CoN673 might be due to Co_3O_4 crystallites sintering at higher temperatures. In agreement with previous reports [18,27,50,51], cobalt reducibility was found to depend on cobalt dispersion. Larger Co_3O_4 crystallites in the CoN673 sample seem to be much easier to reduce than smaller Co_3O_4 crystallites in the CoN373 and CoN423 samples. Both TPR combined with in situ magnetic measurements and XPS of the reduced samples display (Figs. 8 and 9) a higher concentration of cobalt metal phase in the CoN catalysts with larger Co_3O_4 crystallites. The cobalt crystallite size could change during the reduction from Co_3O_4 to metallic cobalt. Indeed, upon reduction of Co_3O_4 to metallic cobalt, XPS shows a decrease in particle size calculated with the use of the Kerkhof–Moulijn model (for CoN423, from 7.5 to 7.2 nm; for CoN673, from 16.8 to 8.4 nm). This observation is in agreement with earlier data of Castner et al. [18].

The number of cobalt metal sites appears to be a function of both cobalt reducibility and cobalt dispersion. The catalyst, which combines high cobalt dispersion and good cobalt reducibility, would therefore have a maximum number of active cobalt metal surface sites. Propene chemisorption shows (Table 1) that the maximum number of cobalt metal sites could be achieved by decomposition of cobalt nitrate at the optimal calcination temperature (423 K). Catalyst oxidative pretreatment at 373 K results in particles of Co_3O_4 that are too small, which are then difficult to reduce, whereas calcination at higher temperatures leads to larger, readily reducible Co_3O_4 crystallites, which do not provide a high concentration of cobalt metal surface sites, however.

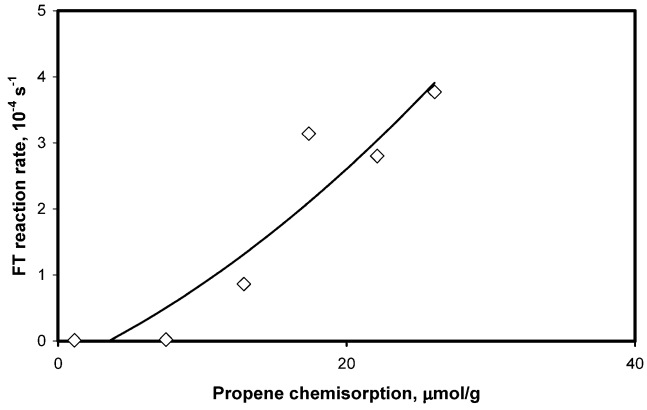

Fig. 12. FT reaction rate as a function of propene chemisorption over cobalt catalysts prepared from cobalt nitrate or cobalt acetate (cobalt loading ∼10 wt%).

Table 2 shows that among the catalysts prepared from cobalt nitrate, the sample precalcined at 423 K exhibits the highest FT activity. This is consistent with a higher concentration of cobalt metal sites in this catalyst found by propene chemisorption. Lower FT reaction rates observed over the catalysts prepared from cobalt nitrate and precalcined at 373 and 673 K were due, respectively, to the presence of inactive unreduced cobalt species and lower cobalt dispersion.

A higher concentration of amorphous, barely reducible cobalt silicate results in lower FT reaction rates over the catalysts prepared from cobalt acetate (Table 2). CoAc catalysts were several times less active in FT synthesis than those prepared from cobalt nitrate. The catalytic activity of CoAc can be still improved. The data show that soft cobalt acetate decomposition leads to an increase in the number of cobalt metal sites. FT reaction rates were more than 10 times higher when the decomposition of supported cobalt acetate was carried out at lower temperatures.

A good correlation for both cobalt-supported silica catalysts prepared from nitrate and acetate is observed between FT reaction rates and the number of cobalt metal sites measured by propene chemisorption (Fig. 12). FT reaction rates seem to be almost proportional to the number of propene chemisorption sites. This finding is consistent with earlier publications. Iglesia et al. [6–8] showed that at the conditions favoring hydrocarbon production, FT reaction rates increase linearly with increasing cobalt dispersion, regardless of the identity of the catalytic support.

Oxidative pretreatment of the catalysts prepared from cobalt nitrate at 373–423 K leads to higher chain growth probability and slightly higher selectivity for methane measured at 7% carbon monoxide conversion (Table 2). Char-

acterization data (Table 1) show that CoN423 and CoN373 catalysts contain smaller and less reducible cobalt particles. Note that the chain growth probability (α) is higher over CoN423 and CoN373 than over CoN673 (Table 2); the somewhat lower C_{5+} selectivity observed over CoN423 seems to be attributable to higher methane selectivity.

Earlier studies of FT synthesis have suggested [57,58] that the sizes of cobalt crystallites could significantly affect the FT reaction rate and hydrocarbon selectivity. The sites of strong carbon monoxide chemisorption were believed to be responsible for the production of heavier hydrocarbons. Thus, one of the possible interpretations of different chain growth probabilities on CoN373 and CoN423 catalysts could be related to the effect of cobalt particle size on the rates of elementary polymerization steps.

In more recent works, however, it was found that the intrinsic chain growth kinetics is not influenced much by the sizes of cobalt crystallites in Co-supported catalysts or by the identity of the support [6–8,54]. Currently there is a consensus in the literature that FT synthesis is not a structure-sensitive reaction, and the rates of chain growth steps are not affected by cobalt dispersion. Kinetic analysis suggests that the higher rate of readsorption of olefins and their subsequent reinsertion into polymerization would decrease the probability of termination via olefin desorption. It would increase the chain growth probability and decrease the olefin/paraffin ratio. The higher chain growth probability and lower olefin/paraffin ratio observed over CoN373 and CoN423 catalysts (Fig. 11, Table 2) could be therefore attributed to the enhancement of secondary reactions such as olefin readsorption and their influence on hydrocarbon selectivity [54,59].

5. Conclusion

It was found that the cobalt precursor and its pretreatment conditions strongly influenced both the structure of supported cobalt species and their catalytic behavior in FT synthesis. After impregnation with cobalt nitrate or acetate, the catalysts indicate the presence of partially dehydrated, octahedrally coordinated cobalt ions. Depending on the pretreatment conditions and the exothermicity of cobalt precursor decomposition, supported cobalt ions either agglomerate into Co_3O_4 crystallites or react with silica, yielding amorphous cobalt silicate. The endothermicity of cobalt nitrate decomposition favors Co_3O_4 crystallites, whereas the exothermicity of cobalt acetate decomposition leads to barely reducible cobalt silicate. The concentration of amorphous cobalt silicate can be minimized by the efficient control of the heat flow at the stage of cobalt acetate decomposition. Endothermic decomposition of cobalt nitrate at relatively lower temperatures leads to higher cobalt dispersion but decreases cobalt reducibility.

The FT reaction rates were found to be a function of the number of cobalt metal sites; a higher concentration of cobalt metal sites in the catalysts prepared via soft decomposition of cobalt nitrate results in the most catalytic activity. It was shown that low-temperature decomposition of cobalt acetate, which increased the concentration of cobalt metal surface sites, could significantly enhance the FT catalytic performance.

Acknowledgments

The authors thank O. Gardoll and R. Bechara for measuring DSC-TGA curves and catalyst BET surface areas. Thanks are due to F. Villain and M. Frère for their assistance in measuring X-ray absorption data and XPS, respectively. The authors gratefully acknowledge the FEDER, CNRS, Nord-Pas de Calais region, and the French Ministry for Higher Education and Scientific Research for their financial support for acquisition of the X-ray photoelectron spectrometer. P.A.C. is thankful for the financial support of his work from the Russian Foundation for Fundamental Research (grant #020332556). The Laboratoire pour l'Utilisation de Rayonnement Electromagnétique (LURE) is acknowledged for the use of beam time.

References

[1] R.B. Anderson, in: The Fischer–Tropsch Synthesis, Academic Press, New York, 1984.
[2] P. Chaumette, Revue IFP 51 (1996) 711.
[3] A. Kiennemann, P. Courty, Actualité Chim. (mai–juin 2002) 31.
[4] M.M.G. Senden, A.D. Punt, A. Hoek, Stud. Surf. Sci. Catal. 119 (1998) 961.
[5] A.C. Vosloo, Fuel Proc. Technol. 71 (2001) 149.
[6] E. Iglesia, Appl. Catal. A: Gen. 161 (1997) 59.
[7] E. Iglesia, S.C. Reyes, R.J. Madon, S.L. Soled, Adv. Catal. 39 (1993) 221.
[8] E. Iglesia, S.L. Soled, R.A. Fiato, J. Catal. 137 (1992) 212.
[9] M. Dry, Catal. Today 71 (2002) 227.
[10] M. Dry, Appl. Catal. A: Gen. 138 (1996) 319.
[11] R. Oukaci, A.H. Singleton, J.G. Goodwin Jr., Appl. Catal. 186 (1999) 129.
[12] I. Puskas, T.H. Fleisch, J.B. Hall, B.L. Meyers, R.T. Roginski, J. Catal. 134 (1992) 615.
[13] K.E. Coulter, A.G. Sault, J. Catal. 154 (1995) 56.
[14] E. van Steen, G.S. Sewel, R.A. Makhothe, C. Micklethwaite, H. Manstein, M. de Lange, C.T. O'Connor, J. Catal. 162 (1995) 220.
[15] A. Khodakov, O. Ducreux, J. Lynch, B. Rebours, P. Chaumette, Oil & Gas Sci. Technol. Rev. IFP 54 (1999) 525.
[16] J.M. Jablonski, M. Wolcyrz, L. Krajczyk, J. Catal. 173 (1998) 530.
[17] D. Schanke, S. Vada, E.A. Blekkan, A.M. Hilmen, A. Hoff, A. Holmen, J. Catal. 156 (1995) 85.
[18] D.G. Castner, P.R. Watson, I.Y. Chan, J. Phys. Chem. 94 (1990) 819.
[19] S. Sun, N. Tsubaki, K. Fujimoto, Appl. Catal. A: Gen. 202 (2000) 121.
[20] A.Y. Khodakov, R. Bechara, A. Griboval-Constant, Appl. Catal. A: Gen. 254 (2003) 273.
[21] A.Y. Khodakov, R. Bechara, A. Griboval-Constant, Stud. Surf. Sci. Catal. 142 (2002) 1133.
[22] A. Griboval-Constant, A.Y. Khodakov, R. Bechara, V.L. Zholobenko, Stud. Surf. Sci. Catal. 144 (2002) 609.
[23] A.Y. Khodakov, A. Griboval-Constant, R. Bechara, V.L. Zholobenko, J. Catal. 206 (2002) 230.

[24] A.Y. Khodakov, A. Griboval-Constant, R. Bechara, F. Villain, J. Phys. Chem. B 105 (2001) 9805.
[25] B.D. Cullity, Elements of X-ray Diffraction, Addison-Wesley, London, 1978.
[26] R.W.G. Wyckoff, Crystal Structures, Interscience, New York, 1960.
[27] A.Y. Khodakov, J. Lynch, D. Bazin, B. Rebours, N. Zanier, B. Moisson, P. Chaumette, J. Catal. 168 (1997) 16.
[28] N. Morimoto, M. Tokonami, M. Watanabe, K. Koto, Am. Mineralogist 59 (1974) 475.
[29] F.P.J. Kerkhof, J.A. Moulijn, J. Phys. Chem. 83 (1979) 1612.
[30] V.V. Kiselev, P.A. Chernavskii, V.V. Lunin, Russ. J. Phys. Chem. 61 (1987) 151.
[31] P. Malet, A. Canallero, J. Chem. Soc., Faraday Trans. I 84 (1988) 2369.
[32] P.A. Chernavskii, A.S. Lermontov, G.V. Pankina, S.N. Torbin, V.V. Lunin, Kinet. Catal. 43 (2002) 268.
[33] P.A. Chernavskii, G.V. Pankina, A.S. Lermontov, V.V. Lunin, Kinet. Catal. 44 (2003) 657.
[34] A.A. Verberkckmoes, B.M. Weckhuysen, R.A. Schoonheydt, Micropor. Mesopor. Mater. 22 (1998) 165.
[35] Y. Okamoto, K. Nagata, T. Adachi, T. Imanaka, K. Inamura, T. Takyu, J. Phys. Chem. 95 (1995) 310.
[36] M.G. Ferreira de Silva, Mater. Res. Bull. 34 (1999) 2061.
[37] J.H. Aschley, P.C.H. Mitchell, J. Chem. Soc. A (1968) 2821.
[38] S.W. Ho, M. Horialla, D.M. Hercules, J. Phys. Chem. 94 (1990) 6396.
[39] T.J. Chaung, C.R. Brundle, D.W. Rice, Surf. Sci. 59 (1976) 413.
[40] T. Cseri, S. Békássy, G. Kenessey, G. Liptay, F. Figueras, Thermochim. Acta 288 (1996) 137.
[41] L. Poul, N. Jouini, F. Fievert, Chem. Mater. 12 (2000) 3123.
[42] M. Zayat, D. Levy, Chem. Mater. 12 (2000) 2763.
[43] J.P. Bonnelle, J. Grimblot, A. D'huysser, J. Electron Spectrosc. 7 (1975) 151.
[44] M. Oku, Y. Sato, Appl. Surf. Sci. 55 (1992) 37.
[45] J.-G. Kim, D.L. Pugmire, D. Battaglia, M.A. Langell, Appl. Surf. Sci. 165 (2000) 70.
[46] V.M. Jiménez, A. Fernández, J.P. Espinós, A.R. González-Elipe, J. Electron Spectrosc. Relat. Phenom. 71 (1995) 61.
[47] D.G. Castner, P.R. Watson, I.Y. Chan, J. Phys. Chem. 93 (1989) 3188.
[48] J. Haber, J. Stoch, L. Ungier, J. Electron Spectrosc. Relat. Phenom. 9 (1976) 459.
[49] S.W. Ho, M. Horialla, D.M. Hercules, J. Phys. Chem. 94 (1990) 6396.
[50] R. Bechara, D. Balloy, J.-Y. Dauphin, J. Grimblot, Chem. Mater. 11 (1999) 1703.
[51] B. Ernst, A. Bensaddik, L. Hilaire, P. Chaumette, A. Kiennemann, Catal. Today 39 (1998) 329.
[52] C.R. Brundle, T.J. Chuang, D.W. Rice, Surf. Sci. 60 (1976) 286.
[53] A. Griboval-Constant, J.-M. Giraudon, G. Leclercq, L. Leclercq, Appl. Catal. A: Gen. 260 (2004) 35.
[54] E.W. Kuipers, I.H. Vinkenburg, H. Oosterbeek, J. Catal. 152 (1995) 137.
[55] A. Martínez, C. López, F. Márquez, I. Díaz, J. Catal. 220 (2003) 486.
[56] H. Ming, B.G. Baker, Appl. Catal. 123 (1995) 23.
[57] L. Fu, C.H. Bartholomew, J. Catal. 92 (1985) 376.
[58] C.H. Bartholomew, R.C. Reuel, J. Catal. 85 (1984) 78.
[59] H. Schulz, M. Claeys, Appl. Catal. A: Gen. 186 (1999) 91.